https://doi.org/10.5194/egusphere-2026-4302
Preprint. Discussion started: 24 July 2026

Physical connectivity and Lagrangian transport patterns in the Bay of Biscay across 30 years

Nadine Steiger[1*], Ivan Manso-Narvarte[1], Ainhoa Caballero[1], Anna Rubio[1]

[1]AZTI, Marine Research, Basque Research and Technology Alliance (BRTA), Herrera Kaia, Portualdea, 20110 Pasaia, Spain

Correspondence to: Nadine Steiger (nsteiger@azti.es)

Abstract. Understanding ocean physical connectivity is essential for characterizing and predicting transport patterns, which in turn play a fundamental role in several marine processes. Here, we present an analysis of 30 years of surface water connectivity for the Bay of Biscay, derived from backward Lagrangian particle simulations driven by hourly high-resolution surface velocity reanalysis fields. The Lagrangian simulations are used to characterize transport pathways within and between key subregions across integration times of 7, 30, and 90 days, thereby capturing connectivity from weekly to seasonal scales.

Results show that the obtained seasonal cycle of connectivity reflects the seasonal variability of regional ocean circulation: i) The northward transport along the shelf by the Iberian–Poleward Current, ii) the presence of transport barriers along the continental slope, and iii) the enhanced cross-shelf transport from the Spanish shelf during spring and from the French shelf during summer. Regional maps of particle origins and transit times reveal areas of strong isolation along the French coast and zones of intensive mixing at the French Spanish border. While interannual variability is evident, the simulations also indicate a slight but significant long-term decrease in transport from the Spanish to the French shelf.

Overall, these results provide an overview of the main pathways of transport and retention within the Bay of Biscay at different time scales, offering insights into its potential role in different key ocean processes such as marine litter or plankton dispersal, genetic exchange, and ecosystem functioning.

1 Introduction

Ocean connectivity is a fundamental process in the marine system. Through the exchange of biogeochemical tracers and other materials, it influences biodiversity, population dynamics, and ecosystem resilience (Cowen and Sponaugle, 2009). Among the physical drivers of connectivity, ocean circulation plays a central role by shaping dispersal pathways, retention areas, and transport barriers. Currents can connect distant habitats by transporting larvae, plankton, and other propagules, while also redistributing environmental DNA (eDNA) and anthropogenic material such as marine litter (e.g. plastics). At the same time, they can limit exchange across fronts, recirculation zones, and other persistent oceanographic boundaries (Lett et al., 2010). As a result, physical connectivity is increasingly recognized as a key factor for understanding both ecological

https://doi.org/10.5194/egusphere-2026-4302
Preprint. Discussion started: 24 July 2026

processes—such as species distribution, recruitment variability, gene flow, and biogeographic structuring—and the transport, dispersion, and accumulation of marine litter (Lebreton et al. 2012; Leis, 2007; Paris et al., 2007; Treml et al., 2015)[NS5.1]. In addition, the relevance of connectivity extends beyond ecological theory, as it directly affects the design and functioning of marine protected area networks, fisheries management, and the capacity of species to respond to climate-driven environmental change (Assis et al., 2021; Gaines et al., 2010; Magris et al., 2014). Indeed, networks designed with connectivity in mind tend to protect more species and functional diversity over the long term, compared to isolated marine protected areas (MPAs) (Balbar and Metaxas, 2019; Magris et al., 2014); and yet, connectivity has often been overlooked in practical spatial planning and fisheries management. Given the central role of connectivity in key marine processes (biodiversity, ecosystem dynamics, the transport of marine litter, etc.), a detailed and systematic understanding of transport pathways and connectivity patterns across spatial and temporal scales within regional seas is essential.

The Bay of Biscay (BoB) provides a particularly relevant setting in which to investigate connectivity patterns. Located in the northeastern Atlantic[NS6.1], the BoB is a transitional region between temperate and subtropical influences and supports productive ecosystems, valuable fisheries resources, and areas of high ecological importance (Borja et al., 2019; Gil, 2008; ICES, 2024). Its physical setting is marked by pronounced spatial heterogeneity, including a broad continental shelf in the north, a narrower shelf along the southeastern margin, and complex bathymetric features (Amaro et al., 2016; Borja et al., 2019). At the open ocean, the circulation is slow with an average anticyclonic sense (Koutsikopoulos and LeCann,1996). Along-slope transport is largely controlled by the Iberian Poleward Current (IPC), which exhibits a pronounced seasonal variability, with a well-defined poleward flow during late autumn and winter and a weaker, more variable behaviour during summer months (Charria et al., 2013; Solabarrieta et al., 2014). Over the continental shelf, circulation is strongly influenced by wind-driven processes, which tend to dominate over tidal and density-driven currents due to the narrow shelf width and the limited river discharge in the region (Charria et al., 2013; González et al., 2004; Solabarrieta et al., 2014). The interaction between the IPC and the abrupt bathymetry, particularly around the Cap Ferret and Capbreton canyon, frequently leads to the generation of mesoscale structures such as eddies (Caballero et al., 2008, 2014, 2016; Pingree and Le Cann, 1992a; Rubio et al., 2018; Teles-Machado et al., 2016), which can significantly modulate transport pathways and residence times.[NS7.1][NS7.2] As a result, surface transport conditions exhibit strong variability across a range of temporal scales, from seasonal to interannual, reflecting the combined influence of large-scale circulation and mesoscale dynamics. These processes favour exchanges among distant sectors of the basin, promote local retention over the shelf, or function as partial barriers between adjacent regions. Indeed, previous observational and modelling studies have shown that transport in the BoB is strongly modulated by seasonality. Surface drifter climatologies indicate a marked seasonal cycle, with poleward shelf–slope transport and IPC intrusions during autumn–winter, and weaker or reversed circulation patterns during spring–summer (Charria et al., 2013). This seasonal modulation also affects residence times over the shelf and slope, as revealed by previous HF radar observations and Lagrangian modelling in the southeastern BoB (Rubio et al., 2018). Numerical simulations further suggest that this seasonality is not limited to the surface but extends through a vertically structured slope-current system, with recurrent reversals and distinct transport regimes within the upper layer, and at intermediate and higher

https://doi.org/10.5194/egusphere-2026-4302
Preprint. Discussion started: 24 July 2026

depths (Friocourt et al., 2007). Lagrangian observations also reveal that mesoscale eddies contribute to exchanges between the slope and the abyssal plain (Rubio et al., 2018; Serpette et al., 2006). More recent high-resolution modelling has quantified these cross-shelf exchanges and shown that they involve distinct vertical layers, with wind forcing, eddy activity and bottom-boundary processes contributing differently to surface, mid-depth and near-bottom transports (Akpınar et al., 2020). Finally, recent studies further show that mesoscale and submesoscale fronts can strongly affect transport pathways and generate transient transport barriers at shorter time scales in the southeastern BoB. These frontal structures modulate the convergence, retention and offshore export of floating material, with their position and persistence strongly influenced by wind forcing and windage effects (Bertin et al., 2024, 2026). Understanding this multi-scale transport framework is essential for interpreting how physical connectivity modulates ecological and environmental processes.

For example, variability in larval retention and offshore export has been shown to influence anchovy (Engraulis encrasicolus) early life stages (Irigoien et al., 2007, 2008; Manso-Narvarte et al., 2024). At larger spatial scales, hydrographic structures near the northern boundary of the BoB have been linked to reduced exchanges with the Celtic Sea and English Channel, contributing to the maintenance of biogeographic transitions in planktonic and other marine communities (Le Marchand et al., 2020; Lett et al., 2010). More recently, connectivity has also been implicated in climate-related range shifts, as changing environmental conditions and transport pathways may facilitate the poleward expansion of species in the northeast Atlantic (Le Marchand et al., 2020; van der Kooij et al., 2024). In addition, the prevailing hydrodynamic conditions drive the accumulation of floating marine litter, thereby identifying the BoB as a hot spot for marine litter (Basurko et al., 2022; Decleck et al., 2019; Pereiro et al., 2019; Ruiz et al., 2022a, b). Moreover, harmful algal blooms and their transport and connectivity have been analysed for the Ostreopsis species between different regions of the BoB, observing that the areas in the middle of the bay favour the algae dispersal towards the north (Drouet et al., 2021).

These studies demonstrate the effects of transport across several types of processes, drifting particles, periods, and regions. However, an overarching view of transport and connectivity patterns across multiple temporal scales and across different areas of the BoB is still lacking. A clear physical description of the BoB circulation is essential as a basis for interpreting connectivity patterns due to exchanges between shelf, slope, and offshore domains, and provides the physical framework needed to understand when connectivity is enhanced, restricted, or redirected across the basin.

In this context, the objective of this study is to characterize transport pathways and physical connectivity among different sub-areas of the BoB. To this end, we use a Lagrangian modelling approach based on numerical particle-tracking simulations forced by ocean surface velocity fields. This framework allows us to quantify exchanges across regions, identify dominant pathways, and assess the spatial and temporal variability of connectivity patterns over 30 years. By relating these results to the main circulation features of the basin, this study aims to provide a physically grounded description of connectivity in the BoB that can support the interpretation of ecological processes and future management applications.

https://doi.org/10.5194/egusphere-2026-4302
Preprint. Discussion started: 24 July 2026

2 Data and Methods

The physical connectivity of different subareas within the BoB is estimated by a Lagrangian model using surface currents from a realistic high-resolution data-assimilating state-of-the-art ocean circulation reanalysis. We quantify transit times, origin of particles, as well as the connectivity and mixing between these subareas within the BoB using different integration times.

2.1 Subareas within the BoB

To evaluate the connectivity patterns, we divide the BoB into subareas that differ in water masses and physical characteristics. For this purpose, we define five main subareas of interest based on the bathymetry contours and the Spanish-French border (Fig. 1): the deep basin (deep, depth > 1000 m) that is characterized by weak mean currents, the presence of eddies and long residence times; the wide French and the narrow Spanish shelf (fr_shelf, es_shelf, depth < 200 m) with currents influenced by wind, tides and river outflows in Region of Freshwater Influence; and the French and Spanish slopes (fr_slope, es_slope, depth = 200–1000 m) that pose topographic barriers to the water exchange between the shelf and the deep ocean. In addition, we define open boundaries to the north (48.5° N), south (41° N), and west (11° W), with particles crossing these limits considered to originate from the respective directions.

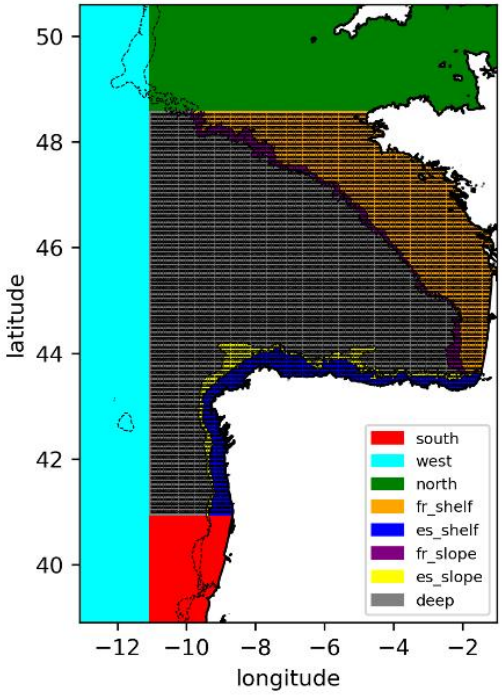

Figure 1: Map of the BoB with colour-coded subareas used for the connectivity (see legend). The dotted grid represents the seeding positions of the particles, and the contours show the 200 and 1000 m isobaths.

https://doi.org/10.5194/egusphere-2026-4302
Preprint. Discussion started: 24 July 2026

The subdivision is motivated by the distinct physical processes operating across the shelf, slope, and deep basin, as well as the contrast between the wide French shelf and the narrower Spanish shelf. However, it should be noted that this classification is to some extent arbitrary with different numbers of particles seeded in each subarea (Table 1) and should be considered when interpreting connectivity patterns. In particular, changes in connectivity between the French shelf and offshore regions largely reflect zonal (west–east) shifts, whereas connectivity associated with the Spanish shelf and slope is influenced by a broader spatial extent that includes parts of the Portuguese coast, resulting in more complex, non-zonal transport pathways.

Table 1: Properties of the subareas in which particles are seeded.

	fr_shelf	es_shelf	fr_slope	es_slope	deep
Bottom depth	< 200 m	< 200 m	200-1000 m	200-1000 m	> 1000 m
Number of seeded particles	1880	460	238	241	5138

2.2 Lagrangian model setup

We use the OpenDrift Lagrangian model (Dagestad et al., 2018; OpenDrift version 1.13.0) to simulate backward trajectories of particles. The model is forced with hourly surface velocity fields from the Atlantic–Iberian Biscay Irish (IBI) Ocean Physics Reanalysis, provided by the Copernicus Marine Service (CMEMS) (https://doi.org/10.48670/moi-00029), covering the period from 1993 to 2024. This product is based on the NEMO v3.6 ocean circulation model run at 1/36° horizontal resolution, and assimilates along-track satellite sea level anomaly, in situ temperature and salinity profiles and satellite sea surface temperature, ensuring a high-resolution representation of the circulation of the BoB.

Particles are seeded on a regular 0.08° x 0.08° grid covering the BoB (41° N to 48.5° N and 11° W to the French and Spanish coastline, see dotted grid in Fig. 1). In each monthly simulation, there are seven particle seeding events spaced five days apart, starting with the 1st of the month as seeding days (Fig. 2). For months with fewer than 31 days, the sequence includes the first day(s) of the following calendar month to maintain seven seedings per month. Each simulation runs backwards in time for 120 days, ensuring at least 90 days of drift for all particles. Simulations were performed for every month of the available velocity data. Each seeding contains 7.958 particles, resulting in a total of 55.706 particles per monthly simulation.

https://doi.org/10.5194/egusphere-2026-4302
Preprint. Discussion started: 24 July 2026

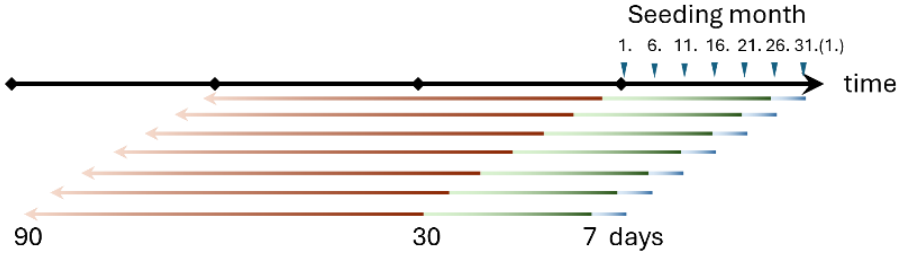

135 **Figure 2: Sketch of the seven seedings within a monthly simulation and 7 (blue), 30 (green), and 90 (orange) days of backward integration.**

The model configuration included no wind drift factor, a diffusion coefficient of zero, and no-stranding conditions (coastline_action = 'previous') to prevent unreal beaching. The particles were forced to move with a time step of 900 s.

140 **2.3 Methodology for Lagrangian metrics**

Since Lagrangian simulations are run backward in time, they reveal the transport pathways and the origin of the particles considering a specified integration time (i.e., age of particles). We focus on integration times of 7, 30 and 90 days to reflect key physical and ecological timescales. The 7-day integration captures short term, event driven transport associated with storms and wind reversals, which can rapidly influence primary production and coastal retention (Wu et al., 2018; Fievet el
145 at. 2026). The 30-day integration corresponds to mesoscale circulation and typical pelagic larval durations (2-4 weeks), making it particularly relevant for functional connectivity between spawning and nursery areas (Ayata et al., 2010; Manso-Narvate et al. 2024). The 90-day integration represents seasonal accumulation of transport pathways, integrating multiple forcing events and reflecting connectivity relevant to population replenishment and ecosystem scale organization (Nadal et al., 2024; Assis et al., 2025).

150 In the following, *seeding positions* refer to the locations where particles are released. The *origin subarea* denotes the subarea occupied by the particle after 7, 30, or 90 days of backward integration, whereas the *seeding subarea* corresponds to the destination subarea in which the particle is seeded (Fig. 1).

To examine seasonal variability, we present results from the simulations of particles seeded during February (winter), May (spring), August (summer), and November (autumn). In the 7- and 30-day simulations, trajectories are influenced only by
155 circulation during the seeding month, whereas the 90-day backward trajectories are influenced by the circulation during the seeding month and the preceding three months (Fig. 2).

We present the following metrics used in the results to analyse how the different subareas of the BoB are connected:

***Particle origin*:** To address the question where particles originate from, we determine the first-, second-, and third-most frequent origin subarea for all particles seeded at each seeding position, considering all seedings per month for monthly

https://doi.org/10.5194/egusphere-2026-4302
Preprint. Discussion started: 24 July 2026

maps and across all years for the climatologies. The first-, second, and third-most frequent origin subareas are calculated as the first, second, and third modes of all possible origins considering different integration times.

***Transit time*:** The transit time represents the time lag (in days) between the particle seeing time and the first entry into each subarea. If a particle never enters a given subarea, this subarea is disregarded for the corresponding particle, whereas the transit time is set to 0 when the particle remains within the same subarea throughout the entire simulation. We then calculate the mean transit time and the standard deviation from each subarea to the seeding positions across all simulations. Because the distance travelled by particles differs among simulations, the number of particles connecting an origin subarea to a given seeding position also varies. To quantify this particle count, we calculate the percentage of particles that reach each seeding position relative to the total number of particles originating from each origin subarea.

Origin diversity index (ODI): To quantify the diversity of particle origins within the BoB, we define the ODI as the number of unique source regions contributing particles to each spatial location. For this, each seeding subarea is divided into a regular grid defined by 100 equally spaced points in longitude and latitude (about 0.12º x 0.12º). For each grid cell, we count the number of unique particle origins present across the seven seeding events per month, separately for the three integration times. Monthly values are then averaged over all available years to obtain a climatological estimate of mixing by season and for different integration times.

Connectivity matrix: We present connectivity matrices that quantify the percentage of particles seeded in each seeding subarea that originate from the different origin subarea. For this, we calculate the connectivity C_{ij} (Eq. 1) between each subarea pair for each integration time T, by counting how many particles seeded within a seeding subarea i originate from each origin subarea j, divided by the total number of particles seeded within the seeding subarea i. This means for each destination subarea i, i.e., each row of the connectivity matrix, the sum is 100 %.

$$C_{ij}^{(T)} = \frac{N_{ij}^{(T)}}{\sum_i N_{ij}^{(T)}} \times 100 \,, \qquad (1)$$

This connectivity matrix is calculated for each monthly simulation and then averaged over all available years to obtain the monthly and overall mean connectivity for the different integration times. Linear trends of connectivity are computed from deseasoned monthly time series of each connectivity *Cij*, where positive trends indicate an increase in connectivity, i.e., an increase in the number of particles transported from an origin subarea to a seeding subarea, whereas negative trends correspond to a reduction in connectivity. Note that the connectivity matrix is not squared as five seeding subareas and eight origin subareas (adding the southern, western and northern boundary) are defined.

Northward extent of Spanish shelf water: We calculate the northward penetration of Spanish shelf water (es_shelf) onto the French shelf as an indication of the strength of the IPC. We use the shelf instead of the slope due to the stronger signal in connectivity and its trend. For each monthly simulation, we extract the positions of particles originating on the Spanish shelf over 90-days integration time. As an estimate of the maximum northward extent, we compute the 99.9th percentile of latitude reached by Spanish shelf particles, which captures episodic far northward intrusions while remaining robust to outliers. We then calculate the monthly climatology of this metric and subtract it from the full time series to obtain monthly anomalies.

https://doi.org/10.5194/egusphere-2026-4302
Preprint. Discussion started: 24 July 2026

These anomalies are used to estimate the long-term trend and to compute annual mean anomalies of the maximum latitude reached by shelf waters. We use a seasonal year (July–June) rather than a calendar year because the northward transport over the shelf peaks during winter and often spans two calendar years. This avoids interpreting shifts in the timing of the winter maximum as changes in magnitude and ensures that the full winter season is included when calculating anomalies in the maximum northward extent of shelf waters.

3. Results

3.1 Particle pathways and origin

The backward Lagrangian simulations provide insights into where seeded particles come from and what their pathways look like. We present here examples of the trajectories of the particles, followed by the seasonal variability of the particle origin.

For a first insight into particle pathways, we illustrate the trajectories from three different months, color-coded by their subarea of origin (Fig. 3, see also trajectories for all years for spring, summer, autumn and winter in Fig. A1, A2, A3). The trajectories exhibit several characteristic circulation features of the BoB: poleward transport of waters from the Portuguese and Spanish shelf (red and blue trajectories); mesoscale eddies over the deep basin (various colors trajectories); lateral import of waters from the western boundary into the basin interior (cyan trajectories); and offshore advection of shelf waters (orange and blue trajectories). The examples selected in Fig. 3 also illustrate the variability across different periods. In particular, they show marked differences in the northward extension of trajectories originating on the Spanish shelf, which is much more pronounced in Fig. 3a and b, as well as in the offshore transport of Spanish slope waters, which occupy the central part of the basin in Fig. 3c. The examples also highlight changes in the position of mesoscale eddies and in the origin of the waters retained within them, as well as differently strong import from the northern boundary. This variability is addressed in more detail on the following using different metrics from a seasonal to interannual scales.

https://doi.org/10.5194/egusphere-2026-4302
Preprint. Discussion started: 24 July 2026

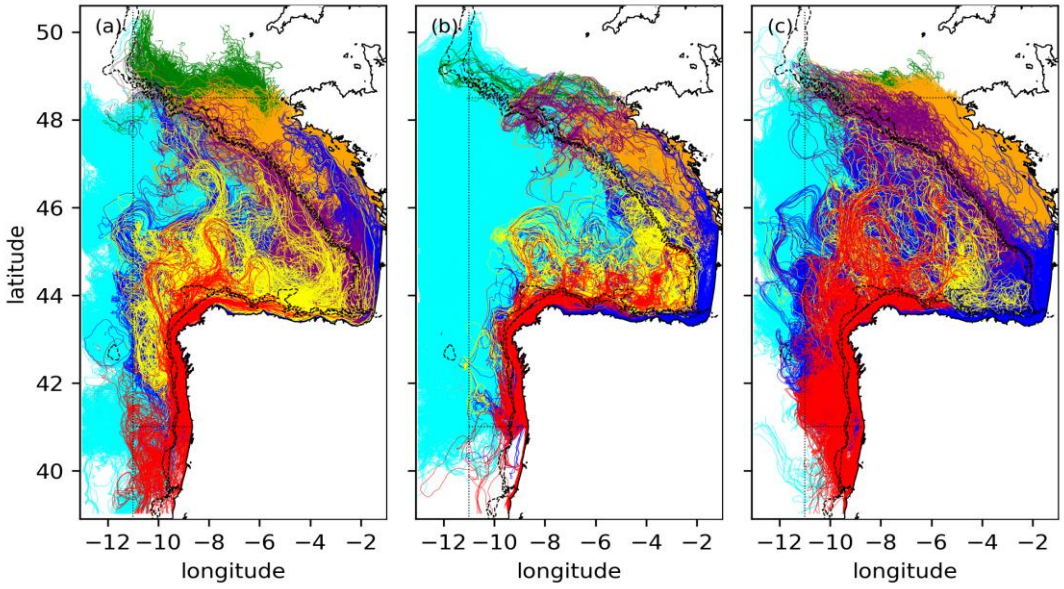

Figure 3: Examples of 90-day backward trajectories of numerical particles seeded throughout (a) November 2015, (b) February 2016, and (c) May 2021. The trajectories are color-coded with their subareas of origin (as defined in Fig. 1) considering 90-days integration time. Contours show the 200 and 1000 m isobaths and dashed lines mark the boundaries between subareas.

To examine the seasonal variability of particle origin, we present monthly climatologies of the particle origin (Fig. 4). Considering the most frequent origin, in winter (Fig. 4a), the western part of the basin is predominantly supplied by particles entering through the western boundary. The French shelf receives particles from the basin interior to about half-way onto the continental shelf, limited contributions from the northern boundary, and inputs from the Spanish shelf in the south. The Spanish shelf and slope are largely occupied by particles from the Spanish shelf, with additional input from the southern boundary in their southernmost part. The particles from the Spanish shelf remain strongly confined by the steep continental slope, but spread northward along the French coast, where they are advected poleward to approximately 45.3° N. In spring (Fig. 4b), retention increases on both the French shelf and in the deep basin, while Spanish shelf particles are transported westward and across the slope and into the basin. The extension to which particles from the western boundary reach into the basin decreases. In summer (Fig. 4c), the northern French shelf is flushed by particles originating at the northern boundary southward to about 47° N, the French shelf particles are exported across the slope into the basin and the Spanish shelf particles are strongly confined except on the western facade of the northern Iberian Peninsula. Northward transport from the Spanish to the French shelf is strongly reduced in summer. In autumn (Fig. 4d), Spanish shelf particles are again strongly confined, with only a narrow northward pathway onto the French shelf, and the northern French shelf is once more supplied by particles from the northern boundary. Across the 30-year dataset and all monthly seedings, slope regions do not appear as a dominant origin in any season, and the southern boundary only appears as a primary origin in winter.

Considering the second-most frequent origin (Fig. 4e-h), the smaller slope regions with less particles remain absent for the 90-day integration time, reflecting the strong dispersal and weak coherent imprint of these pathways. However, in this mode, particles from the southern boundary are more prominent and their northward pathway along the Spanish coast reach as far

https://doi.org/10.5194/egusphere-2026-4302
Preprint. Discussion started: 24 July 2026

as 6° W, while particles originating on the Spanish shelf are transported northward along the entire French coast up to about 48° N. A detailed analysis of the northward transport of Spanish shelf waters along the coast will be presented later. The deep basin is primarily supplied by particles from the western boundary and from shelf regions.

Particles originating from the slope regions only become prominent as a second-most frequent origin (Fig. 4i-l), where particles from the French slope travel westward into the northern part of the basin, while the Spanish slope particles accumulate in clusters over the Spanish slope that move seasonally. With decreasing integration time, the contribution of slope-origin particles increases. At 30 years, they cover most of the deep basin as the most or second-most frequent origin (Fig. A4), whereas at 7 years they dominate the regions surrounding the slope (Fig. A5). Notably, at the 7-year integration time, an alternating pattern emerges off the Spanish shelf, with both shelf- and slope-origin waters appearing as the third-most frequent origin. The northward extension of Spanish shelf waters along the French coast is mainly expressed as a second-most frequent origin at all integration times.

https://doi.org/10.5194/egusphere-2026-4302
Preprint. Discussion started: 24 July 2026

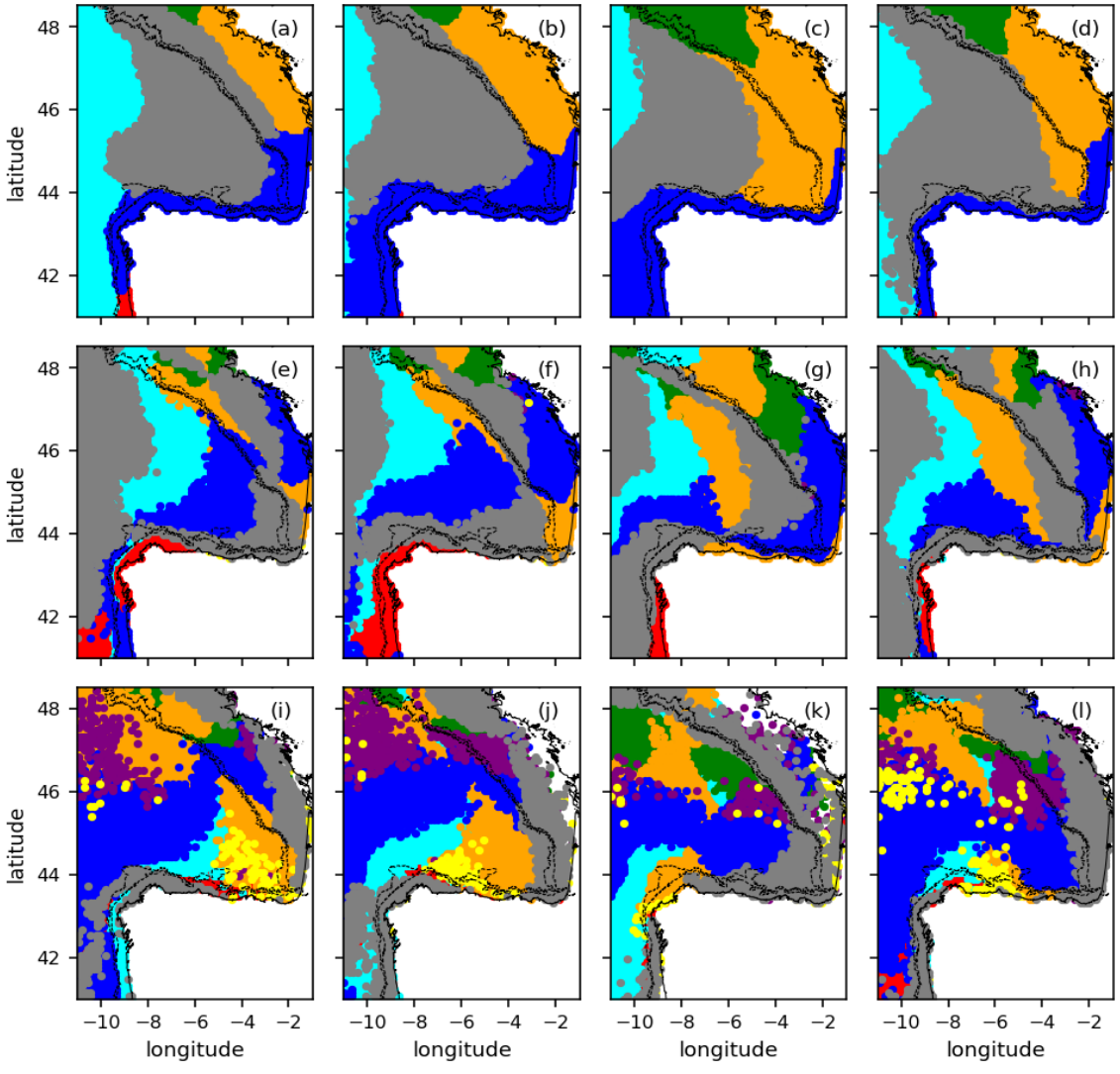

Figure 4: Most frequent (a–d), second-most frequent (e–h), and third-most frequent (i–l) particle origins at each seeding position for particles released in February (representative of winter; a, e, i), May (spring; b, f, j), August (summer; c, g, k), and November (autumn; d, h, l). Colours indicate the origin subarea after 90-day backward simulations, based on the subareas defined in Fig. 1. Light grey contours show the 200 and 1000 m isobaths.

3.2 Transit times and mixing of particle origin

In this section, we characterize particle connectivity using two metrics: the mean transit time between seeding positions and origin subareas, and the ODI, which quantifies the mixing of distinct particle origins. The transit times provide insight into the efficiency of transport between origin subareas and seeding positions. In general, seeding positions are reached more rapidly when they are located close to the origin subarea or connected to it by strong and persistent currents (Fig. 5). Within

https://doi.org/10.5194/egusphere-2026-4302
Preprint. Discussion started: 24 July 2026

seven days (blue colours), particles remain within their origin subarea when averaged over the full period. After 30 days (green colours), particles typically disperse by approximately 1° in longitude and latitude from their origin subarea, with larger distances travelled in specific regions. Notably, particles originating from the Spanish shelf and slope reach farther north over the French shelf than elsewhere along the Spanish coast, while particles originating from the northern boundary extend farther south over the central French shelf than over deeper offshore regions. Within 90 days (orange colours), particles can traverse more than half of the BoB. This includes trajectories extending from the southern boundary beyond 47º N (Fig. 5a), as well as particles originating from the western boundary crossing the French slope and reaching onto the shelf (Fig. 5b). However, such far transport is limited to a small fraction of the ensemble: 90 % of all particles remain within 2–5° of their subarea of origin over the 90-day period. For example, 90 % of particles originating from the southern boundary remain south of 44.5° N (Fig. 5a), while 90 % of those originating from the northern boundary remain north of 47.5° N after 90 days (Fig. 5c). Note that there is a strong variability in transit times, with a standard deviation of up to 35 days, especially in regions that are prone to eddies, such as offshore the shelf regions and where the Spanish shelf water is transported northward (Supplementary Material, Fig. 16). Some locations are not reached at all within 90 days in any of the simulations; in particular, parts of the French coastline do not receive particles originating from the southern, western, or northern boundaries.

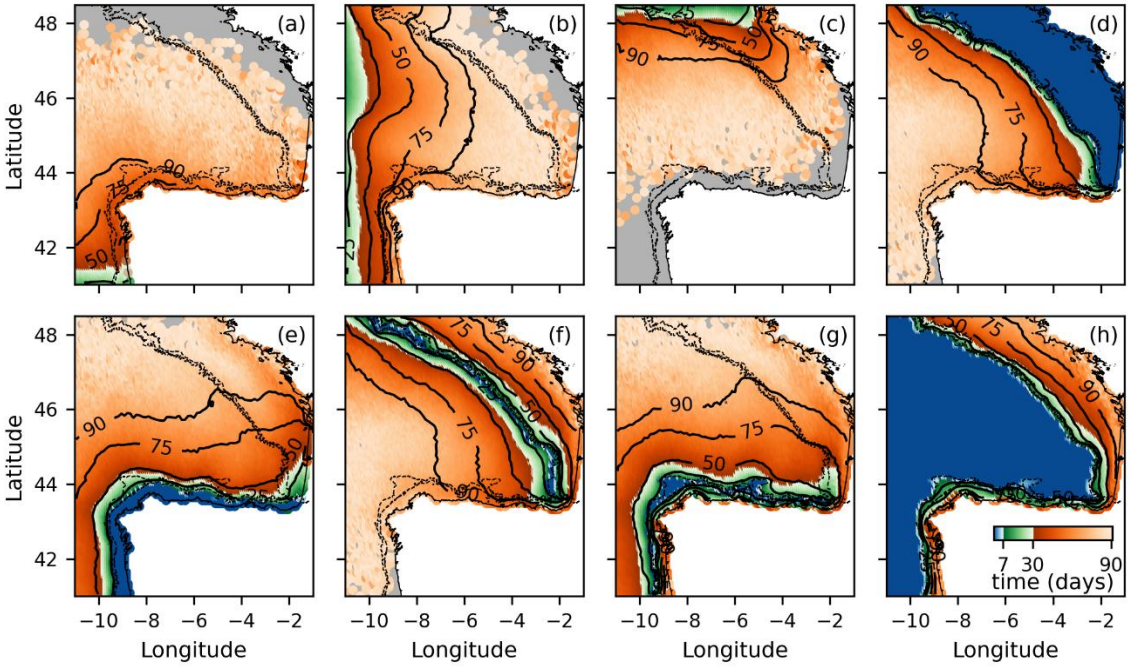

Fig. 5: Maps of mean transit times (days) to the seeding positions for particles originating in the subareas (a) south, (b) west, (c) north, (d) fr_shelf, (e) es_shelf, (f) fr_slope, (g) es_slope, and (h) deep. Blue shades indicate transit times of up to 7 days, green shades up to 30 days, and orange shades up to 90 days. Grey areas indicate locations not reached by particles from the corresponding origin subarea within 90 days. Thick black contours indicate the percentage of particles reaching each location from the corresponding origin subarea within 90 days. Light grey contours denote the 200 and 1000 m isobaths.

https://doi.org/10.5194/egusphere-2026-4302
Preprint. Discussion started: 24 July 2026

The ODI reveals the regions of stronger isolation versus regions with particles of multiple origin or stronger mixing, under the assumption that stronger mixing is associated with a greater diversity of origins (Fig. 6). For an integration time of seven days (Fig. 6a, d, g, j), the ODI is highest near the boundaries between subareas, as expected, with ODI=5 in the southeastern BoB, where particles originating from five different subareas converge. While this pattern is constrained by the definition of the subareas, a clear seasonal variability emerges. The region of largest origin diversity extends farther onto the French shelf during autumn and winter, whereas in spring and summer it shifts westward along the Spanish slope. This seasonal signal becomes more pronounced for a 30-day integration time (Fig. 5b, e, h, k). In this case, regions with ODI=5 near the French Spanish border migrate from the southern French slope in winter, to the southeastern corner of the BoB in spring, to the northeastern Spanish slope in summer, and the southern French shelf in winter. Larger origin diversity is also observed along the western Spanish slope during winter and autumn. In contrast, regions of weak mixing, indicated by a single origin and, thus, strong isolation, are found over the central French shelf from winter to summer, and within the central basin during summer and autumn. For a 90-day integration time (Fig. 5c, f, i, l), particles throughout the basin and over the slopes show ODI=5, with up to ODI=6 in the central basin. The location of this maximum varies seasonally, following the seasonal cycle of the regional ocean circulation. Note that, while eight subareas of origin are defined within the BoB, the maximum ODI observed at any location and for any integration time is six. This reduction results from the diminished contribution of slope regions in the long-term averages (Fig. 4).

https://doi.org/10.5194/egusphere-2026-4302
Preprint. Discussion started: 24 July 2026

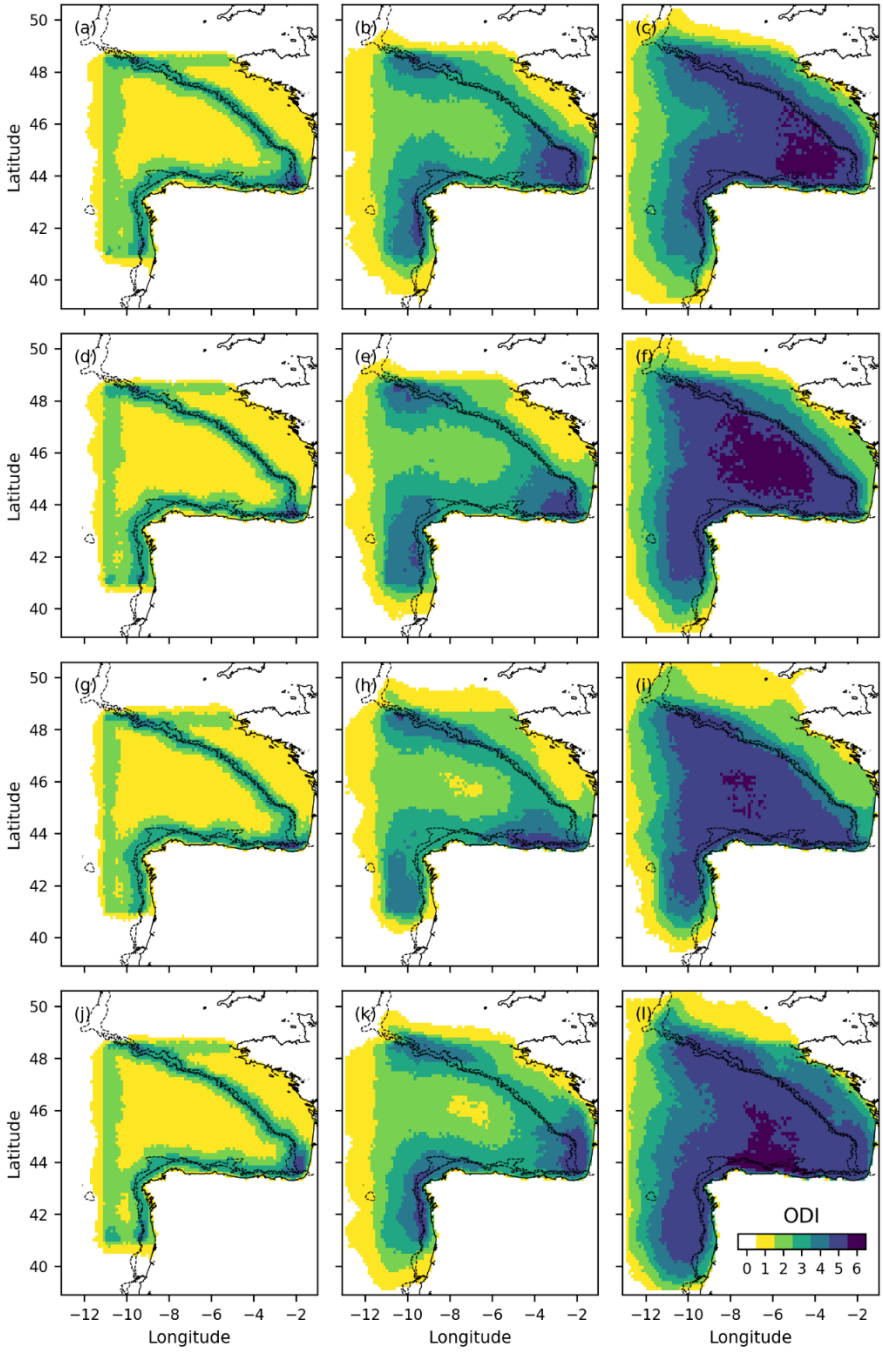

Figure 6: Heat maps of the origin diversity index (ODI, number of unique origins) for gridded bins of approximately 0.12° × 0.12°. Panels show integration times of 7 days (a, d, g, j), 30 days (b, e, h, k), and 90 days (c, f, i, l) for particles seeded in February (representative of winter; a–c), May (spring; d–f), August (summer; g–i), and November (autumn; j–l). Light grey contours denote the 200 and 1000 m isobaths.

https://doi.org/10.5194/egusphere-2026-4302
Preprint. Discussion started: 24 July 2026

3.3 Physical connectivity and its seasonal cycle

To compile the connectivity between all origin and seeding subareas, we present the full connectivity matrix averaged over the entire time period (Fig. 7). After 7 days of integration time (Fig. 7a), strong retention is observed on the shelf regions and in the deep basin, with 89 %, 78 %, and 88 % of particles remaining in the French shelf, Spanish shelf, and deep basin, respectively. In contrast, retention within the slope subareas is much weaker: only 22–23 % of particles remain there, while the majority are transported to adjacent shelf subareas or into the basin. As the integration time increases, particle dispersion intensifies and connectivity between distinct subareas increases. After 30 days (Fig. 7b), retention remains relatively high on the shelves (72 %) and in the deep basin (69 %), whereas the remaining particles predominantly originate from the deep basin and neighbouring subareas or boundaries. After 90 days (Fig. 7c), mixing is substantially enhanced and particle origins become more diverse in agreement with the ODI (Fig. 6). The highest retention rates remain on the shelves, with 69 % and 56 % of particles remaining in the Spanish shelf, and French shelf, respectively. The French shelf and slope receive particles originating from the northern boundary, the deep basin, and the Spanish shelf. The Spanish shelf is connected to particles from the southern boundary, the deep basin, and the French shelf, while the Spanish slope receives particles from the Spanish shelf, deep basin, French shelf, and southern boundary. In particular, the French shelf receives 19 % of particles through the northern and western boundaries and the Spanish shelf receives 17 % of particles from the southern and western boundaries. The deep basin is primarily connected to particles originating from the deep basin itself, the western boundary, and the shelves.

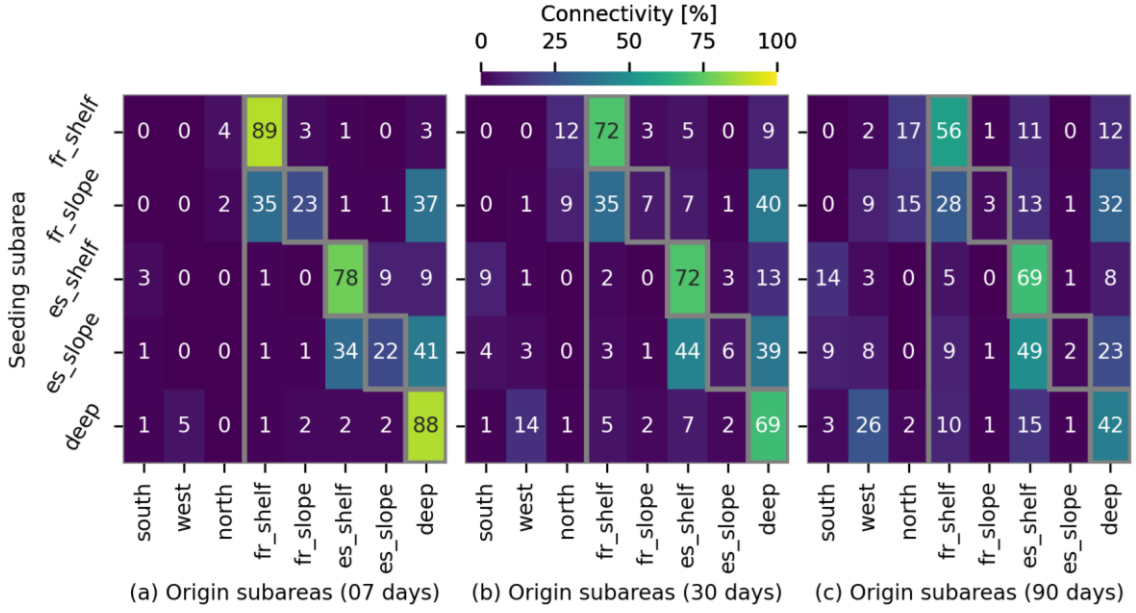

Figure 7: Connectivity matrix showing the percentage of particles seeded in each seeding subarea (y-axis) that originated from each source subarea (x-axis) for integration times of (a) 7 days, (b) 30 days, and (c) 90 days. Values are averaged across all seedings between 1993 and 2024. Grey boxes denote the matrix diagonal, representing particle retention within the same subarea.

https://doi.org/10.5194/egusphere-2026-4302
Preprint. Discussion started: 24 July 2026

Monthly climatological averages of the connectivity (Fig. 8) show that retention on the French and the Spanish shelf is strongest during May and June, while retention in the basin or on the slopes does not show any seasonality. Connectivity from the basin to the French slope and shelf is smallest during July and August, when also the transport from the Spanish shelf to the French coast weakens, while the transport from the northern boundary onto the French shelf and slope peaks one month later (August to September). Accordingly, the transport from the French slope and shelf onto the Spanish slope and shelf is also strongest during summer, while the connectivity from the southern boundary towards the Spanish shelf and slope is weakest during summer. Off-shelf transport from the Spanish shelf to the Spanish slope and the basin is largest during early summer (63 % connectivity from Spanish shelf to slope in June), while the off-shelf transport from the French shelf towards the basin is the largest during September (24 %).

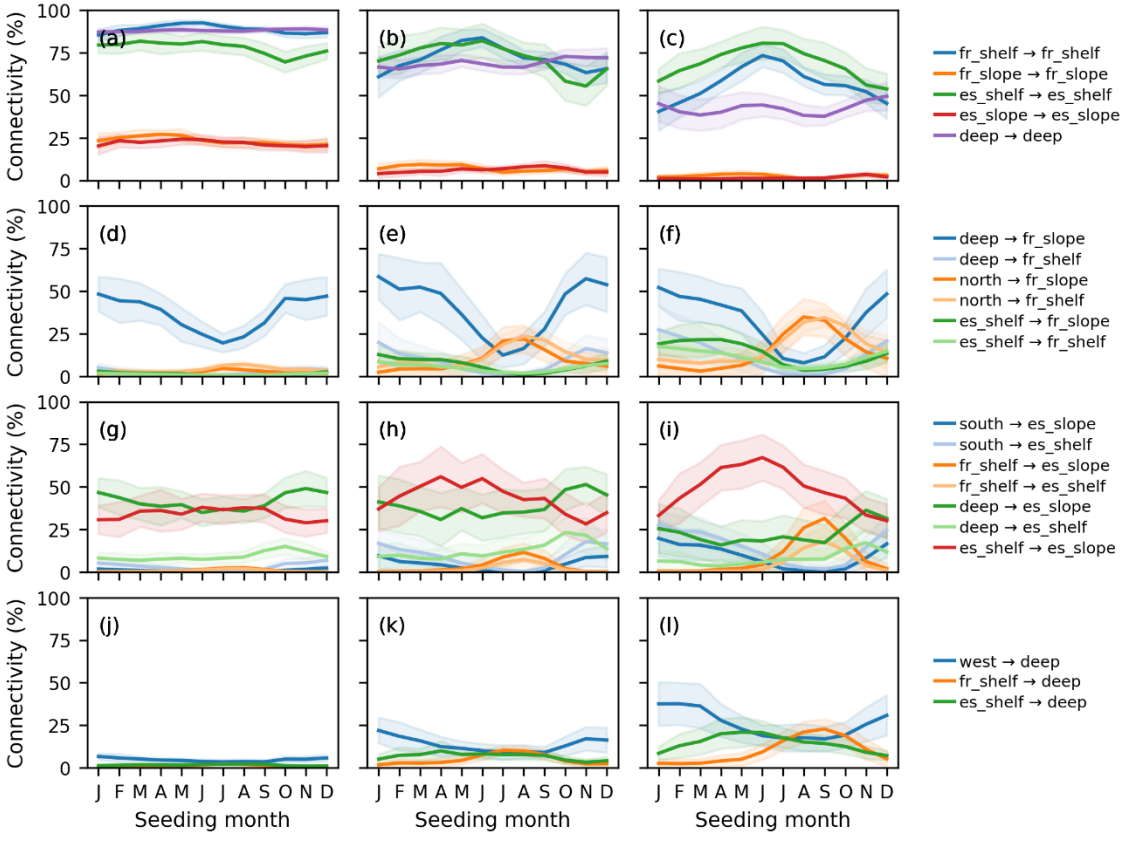

Figure 8: Seasonal cycle of connectivity between subareas for integration times of 7 days (a, d, g, j), 30 days (b, e, h, k), and 90 days (c, f, i, l). Solid lines show the climatological monthly mean connectivity, while shaded areas indicate ±1 standard deviation. For clarity, connections are grouped into retention within subareas (a–c), connectivity with the French shelf and slope (d–f), connectivity with the Spanish shelf and slope (g–i), and connectivity with the deep basin (j–l). Only connections exceeding 3% in the 90-day connectivity matrix (Fig. 7) are included here.

https://doi.org/10.5194/egusphere-2026-4302
Preprint. Discussion started: 24 July 2026

3.4 Long-term trend in connectivity and along-shelf transport

We present the long-term trend in connectivity to reflect changes that have occurred in the BoB over the last 30 years (Fig. 9). For an integration time of seven days (Fig. 9a), trends are small, but they already reveal emerging spatial patterns. Positive trends are detected in the connectivity from the deep basin towards the Spanish shelf and slope, as well as between the French shelf and the French slope. Retention slightly increases over the French shelf and slope and decreases over the Spanish shelf and slope. For longer integration times, the trend patterns become more pronounced. The strongest statistically significant trends correspond to increased connectivity from the basin to the Spanish slope and shelf for the 90-day integration time (Fig. 9c), with rates of 0.013 % month^{-1} and 0.008 % month^{-1}, respectively. Although these monthly trends are small, they to total increases of approximately 4.7 % and 2.9 % in connectivity accumulate over the full 30-year period. In addition, there is a significant negative trend in connectivity from the Spanish shelf to the French shelf and slope (0.006 and 0.007 % month^{-1}, respectively) and from the southern boundary to the Spanish slope and the deep basin (0.007 and 0.002 % month^{-1}, respectively).

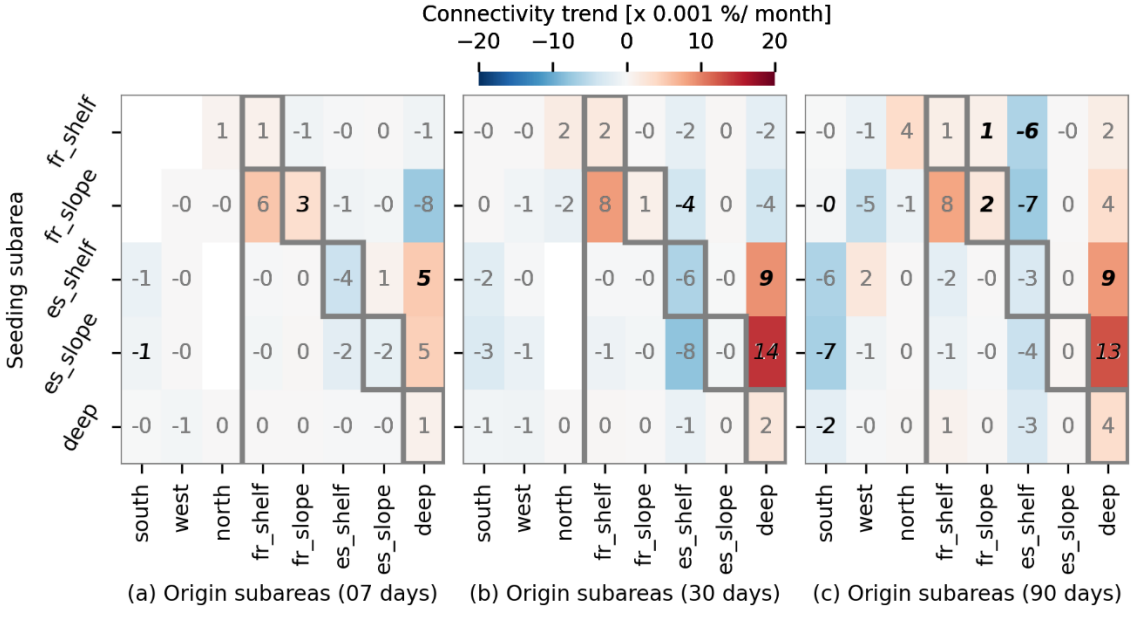

Figure 9: Long-term trend over the entire time period of the deseasoned connectivity in % month^{-1} between each for integration times of (a) 7 days, (b) 30 days, and (c) 90 days. In italic are the trends that are statistically significant on a 95 % confidence level and in italic bold are the trends that are statistically significant on a 99 % confidence level. Grey boxes denote the matrix diagonal, representing particle retention within the same subarea.

With the aim of assessing whether there have been any interannual changes or trend in the northward transport of waters along the coast, we present the variability in the northward extent of the Spanish shelf water. The latitudinal extent of Spanish shelf water exhibits a pronounced seasonal signal (Fig. 10a). On average, the northward extent reaches its minimum value of 46.5° N in August and its maximum value of 47.8° N in November. After removal of the seasonal cycle, the deseasoned monthly anomalies reveal a monthly variability of approximately ±1° latitude (Fig. 10b). Over the full 30-year

https://doi.org/10.5194/egusphere-2026-4302
Preprint. Discussion started: 24 July 2026

period, a statistically significant negative linear trend of −0.0006° N month^{-1} is detected (p = 0.015, 95 % confidence level), indicating a long-term reduction in the northward penetration of Spanish shelf waters. In addition to the overall negative trend, the time series of yearly anomalies reveals a marked change in behaviour around 2012/13 (Fig. 10c). The year 2012 corresponds to the strongest negative anomaly in the entire record, after which the northward extent of the Spanish shelf shows a partial recovery.

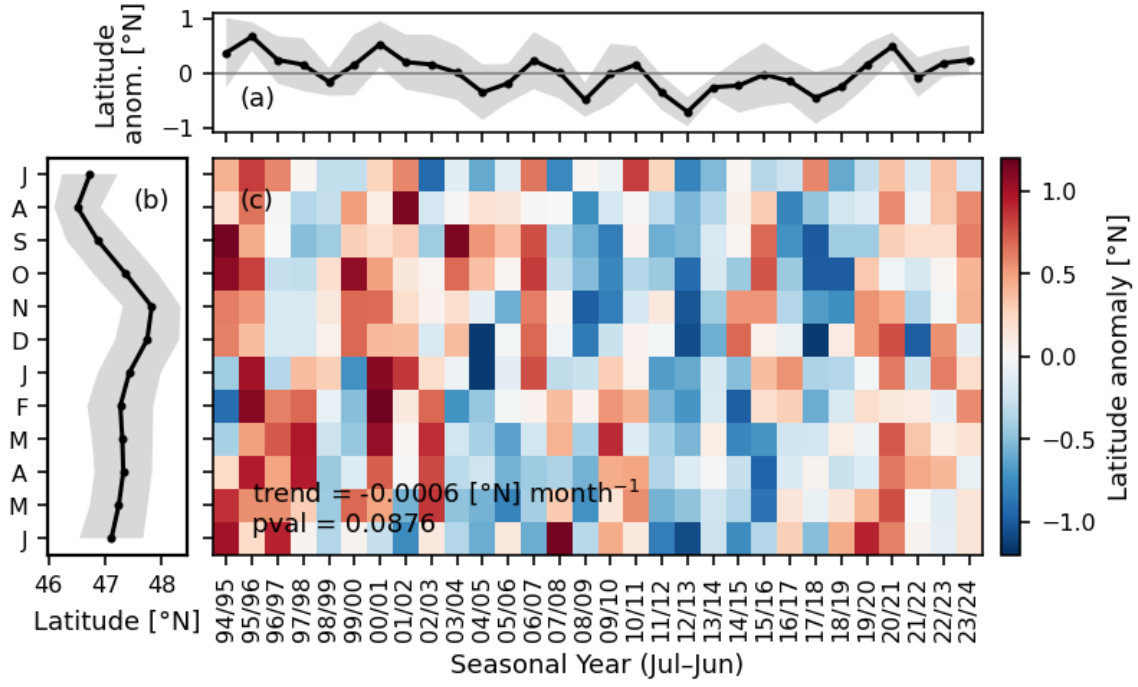

Figure 10: Maximum latitude (99.9th percentile of latitude) of Spanish shelf (es_shelf) waters after 90 days of integration. (a) Climatological seasonal cycle of the maximum latitude, with ±1 standard deviation (grey shading); (b) Hovmöller diagram of anomalies relative to the seasonal cycle, organized by seasonal year (July–June); and (c) seasonal-year mean anomalies, with ±1 standard deviation (grey shading) calculated from the monthly anomalies within each July–June period. Seasonal years are labeled by their starting year (e.g., 94/95 denotes July 1994–June 1995). Months and seasonal years correspond to the particle seeding time.

4. Discussion

The availability of a 30-year time series of marine current velocities enables the assessment of short-term, monthly, seasonal and interannual variability, as well as the calculation of climate trends. Thus, this unique set of long-term Lagrangian simulations with different integration times provides a robust framework for investigating mean patterns, seasonal variability, and long-term changes in transport, mixing, and connectivity within the BoB.

The simulations used in this work are constrained to surface velocities for a twofold reason. First, surface currents are available at hourly resolution, whereas subsurface velocity fields are only available at daily resolution, reducing the ability of the Lagrangian simulations to resolve short-term variability. Moreover, extending the simulations to fully three-dimensional

https://doi.org/10.5194/egusphere-2026-4302
Preprint. Discussion started: 24 July 2026

velocity fields would substantially increase computational costs while introducing additional uncertainties associated with vertical mixing and poorly constrained subsurface flows. Second, surface velocities are the most representative of the horizontal transport of many passive tracers, such as floating marine litter, biomass, planktonic organisms, and eDNA, whose dispersal is largely governed by near-surface advection and Lagrangian transport processes (Andruszkiewicz et al., 2019; Bjorkstedt and Roughgarden, 1997; Prants, 2025; van Sebille, 2020). Nevertheless, there is growing interest in resolving subsurface connectivity for processes in which transport is not restricted to the surface layer, such as the dispersal of early life stages of some pelagic fish and other organisms with more complex behaviors in the water column. This is particularly relevant for species such as European anchovy, whose early life stages may occur below the surface layer, for instance around 20–30 m depth, and whose dispersal can therefore be affected by currents that differ from those at the surface. Previous studies have shown that transport regimes in the BoB can be vertically structured, with surface and subsurface circulation potentially becoming decorrelated across different layers and time scales (Akpınar et al., 2020). Addressing these processes will require continued efforts to improve the spatial and temporal resolution of ocean simulations and available velocity products, together with a better representation of subsurface currents and the vertical component of transport. This implies advancing both numerical models and observing systems capable of constraining subsurface and vertical circulation more accurately.

Overall, our results highlight the complexity and variability of transport and connectivity patterns in the BoB across multiple temporal scales. At seasonal scales, connectivity is strongly modulated by the regional circulation, with alternating periods of enhanced retention, along-shelf transport, cross-shelf exchange, and mixing between shelves, slope and deep-basin waters. At longer time scales, the 30-year simulations reveal that these recurrent seasonal patterns are superimposed on marked interannual variability and on weaker but detectable long-term changes. This multi-scale behavior emphasizes that connectivity in the BoB cannot be described by a single dominant pathway but rather results from the combined influence of persistent circulation features, episodic mesoscale processes, and long-term changes in transport regimes. Overall, the obtained patterns are consistent with the main circulation features and variability previously described for the BoB, including the seasonal modulation of along-shelf transport, shelf retention, cross-shelf exchange and mesoscale activity. However, the patterns depend on the velocity fields used to drive the Lagrangian simulations and should therefore be interpreted in the context of the selected ocean circulation product. Here, we use the most recent Copernicus Marine surface velocity product available at the time of the analysis (1/36° horizontal resolution; released in November 2025), which combines high spatial resolution with data assimilation and currently provides the best available description of surface circulation in the BoB. This product is expected to improve the representation of mesoscale circulation and cross-shelf exchanges relative to the previous 1/12° product, primarily through its finer resolution and enhanced assimilation of altimetric observations. Nevertheless, for smaller-scale applications, such as the analysis of frontal structures or specific transport events, closer validation against local observations remains essential, as illustrated by recent studies combining high-frequency radar and satellite data in the southeastern BoB (Bertin et al., 2024).

https://doi.org/10.5194/egusphere-2026-4302
Preprint. Discussion started: 24 July 2026

The simulations also show that increasing integration time reveals larger origin diversity and connectivity, linked to a larger exchange of particles between subareas. Nevertheless, the French and Spanish shelf subareas consistently show the lowest origin diversity and highest retention rates, likely linked to the IPC, which acts as a dynamical boundary limiting cross-shelf exchanges. In fact, the lowest transport from the shelves to the deep ocean coincides with increased transport from the southern boundary northward along the coast in winter (Fig. 8), agreeing with the strongest IPC period (Charria et al., 2013; Solabarrieta et al., 2014). During summer, when the IPC weakens, this northward transport weakens and transport from the northern boundary towards the French shelf becomes more important. These patterns are consistent with the seasonal cycle of the IPC and previous observations of marine litter patterns in the southeastern BoB (Declerck et al., 2019). The relaxation of the IPC and the subsequent development of mesoscale eddies along the slope in winter (Caballero et al., 2008, 2014, 2016; Pingree and Le Cann, 1992a; Rubio et al., 2018; Teles-Machado et al., 2016) may further enhance exchanges between shelves, slope, and deep-basin waters. However, these kinds of processes deserve specific analyses (e.g. Akpınar et al., 2020) which are out of the scope of our present paper.

It should also be noted that the connectivity patterns reported here partly depend on the choice of subareas used in the analysis. Although expressing connectivities as percentages relative to the number of particles released in each subarea reduces biases associated with unequal numbers of seeded particles (Table 1), it does not account for differences in the size and geometry of the subareas themselves. This is particularly relevant for the slope regions, which are relatively narrow and therefore allow particles to leave the subarea more rapidly than in broader shelves or the deep basin. We nevertheless adopted physically meaningful subareas based on the major hydrographic domains of the Bay of Biscay rather than subdivisions of equal area, as our objective was to investigate connectivity between oceanographically distinct environments. Likewise, we deliberately avoided defining subareas from community maps in order to keep the framework applicable to a broad range of tracers and management questions. Future studies could complement this approach by defining regions based on connectivity communities and comparing the resulting connectivity patterns with those obtained from the physically based subdivision used here.

In addition to the pronounced interannual variability in the northward penetration of Spanish shelf waters, this northward transport shows a long-term decline (Fig. 9). At the same time, transport from the deep basin towards shelf subareas increases (Fig. 8), suggesting that the reduced northward transport may be linked to a weakening of IPC, which in turn reduces the dynamical barrier along the slope and enhances exchange between shelf and deep-basin waters. However, this hypothesis requires further analysis. The reversal of this declining trend around 2012 may be consistent with the large-scale circulation changes in the eastern North Atlantic. In particular, González-Pola et al. (2025) reported a decade-long flow reversal in the intergyre region starting in 2013–2014 that modified density structures and slope circulation in the BoB, weakened upwelling, and altered regional transport pathways, before a gradual return toward the classical circulation regime. This transition may have contributed to the observed partial recovery of northward transport along the shelf. Additional anomalous events were also identified from drifter observations over the Armorican shelf between October 2007 and March 2008, during which cross-shore circulation dominated in place of the typically observed poleward flow (Charria et al., 2013).

https://doi.org/10.5194/egusphere-2026-4302
Preprint. Discussion started: 24 July 2026

The strong retention and limited connectivity simulated over the French and Spanish shelves suggest that these regions may function as relatively isolated hydrographic and ecological compartments. Such isolation can influence both the distribution of water masses and their associated properties (e.g., temperature and salinity) and the transport of drifting particles. Regarding floating marine litter, there is clear evidence that the southeastern BoB acts as an accumulation zone, influenced by regional circulation patterns and riverine inputs (Alfaro-Ortega et al., 2025; Ruiz et al., 2022b). For early life stages of pelagic species, this retention is particularly relevant during and shortly after the spawning season. Species such as the European anchovy spawn mainly along these shelves, especially in areas influenced by major river mouths, during spring and summer (Motos et al., 1996). The early life stages of this species remain pelagic for approximately 20 days (Aldanondo et al., 2008, 2010; Cotano et al., 2008), during which they are transported by near-surface currents and subsequently can be aggregated (Manso-Narvarte et al., 2024). Recruitment success strongly depends on survival during this phase, which is closely linked to environmental conditions and their variability. According to the results of this study, on average, around 50 % of shelf particles remain within this region after one month, except for the southeastern corner of the BoB (Fig. 5). Nevertheless, at a seasonal scale, and compared to other seasons, there is a greater dispersion of shelf surface waters during spring and summer toward the deep basin (Fig. 4), which could induce an offshore transport of these species, thus affecting their early life stages (Irigoien et al., 2007).

To emphasize robust and transferable information, we primarily present climatological and annual or seasonal mean connectivity patterns. These provide a first-order view of typical pathways, retention zones, and exchange regions. As averaging smoothens episodic and mesoscale variability, all the plots for every monthly simulation, the three integration times, including monthly or yearly averages, have been made available through a web application to allow the reader to explore the variability of the Lagrangian metrics in more detail beyond what is shown in this paper.

5. Conclusions

This study delivers a long-term, spatially explicit assessment of physical connectivity for the BoB derived from 30 years of Lagrangian simulations. By resolving connectivity across multiple integration times, the results provide a coherent framework to characterize how transport pathways, retention zones, and exchange regions organize surface-driven connectivity from weekly to seasonal scales. The resulting patterns highlight contrasts between strong dispersion over the Spanish and French slopes and persistent retention on the shelves, including pronounced isolation of the central French shelf. In addition to connectivity matrices, the results offer quantitative transit time information from key subareas, enabling direct application to ecosystem-based management. These metrics provide scientifically based guidance for assessing a wide range of processes, such as potential replenishment pathways of fish stocks, interpreting spatial signals from eDNA observations, and contextualizing biological and environmental connectivity within the regional circulation. The analysis further reveals a

https://doi.org/10.5194/egusphere-2026-4302
Preprint. Discussion started: 24 July 2026

clear seasonal cycle of connectivity and a slight long-term weakening of the northward transport over the shelf combined with increased off-shelf transport.

Overall, this overview of Lagrangian connectivity within the BoB, together with the associated web application, provides a flexible and accessible resource for ecosystem research and management in the BoB. This tool enables scientists, fisheries managers, and other stakeholders to access and visualize connectivity information at spatial and temporal scales relevant to ecosystem management and conservation planning, as well as the interpretation of emerging observation techniques such as eDNA. Beyond its immediate applications, the connectivity framework constitutes a robust, long-term reference for advancing our understanding of physical connectivity under a highly dynamic circulation regime and provides a quantitative basis for supporting sustainable management of marine ecosystems in the BoB.

Appendix A

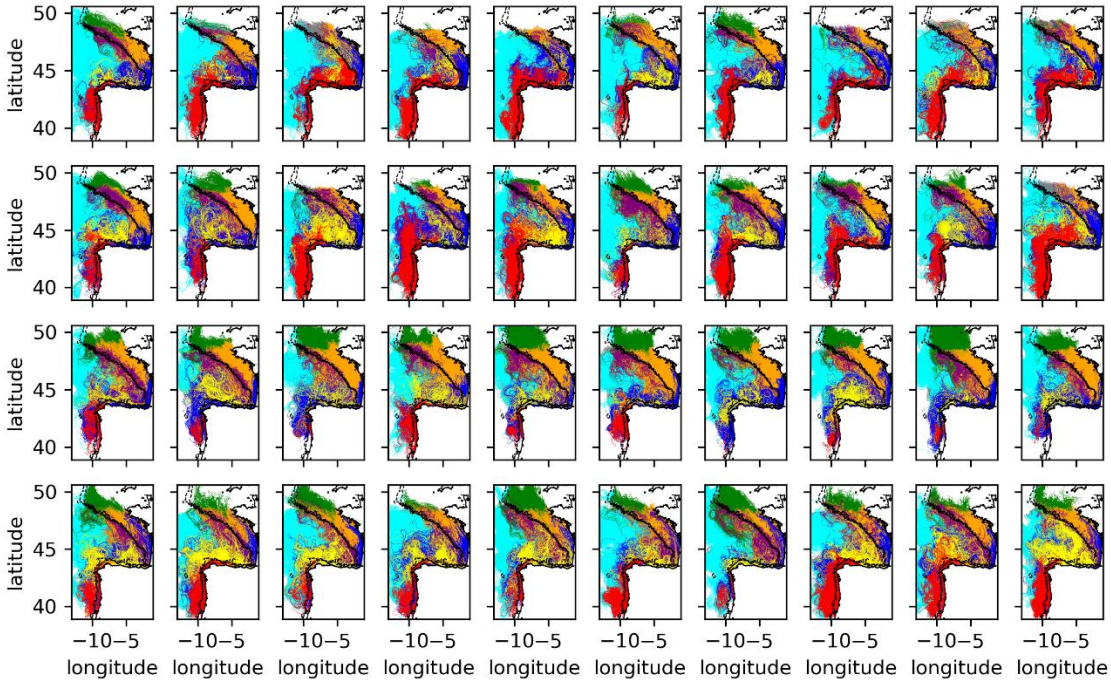

Figure A1: 90 days of backward trajectories of numerical particles seeded throughout February (upper row), May (second row), August (third row) and November (last row) for 1994 – 2003 (left to right). The trajectories are color-coded with their subareas of origin (as defined in Fig. 1) considering 90-days integration time. Contours show the 200 m and 1000 m isobaths.

https://doi.org/10.5194/egusphere-2026-4302
Preprint. Discussion started: 24 July 2026

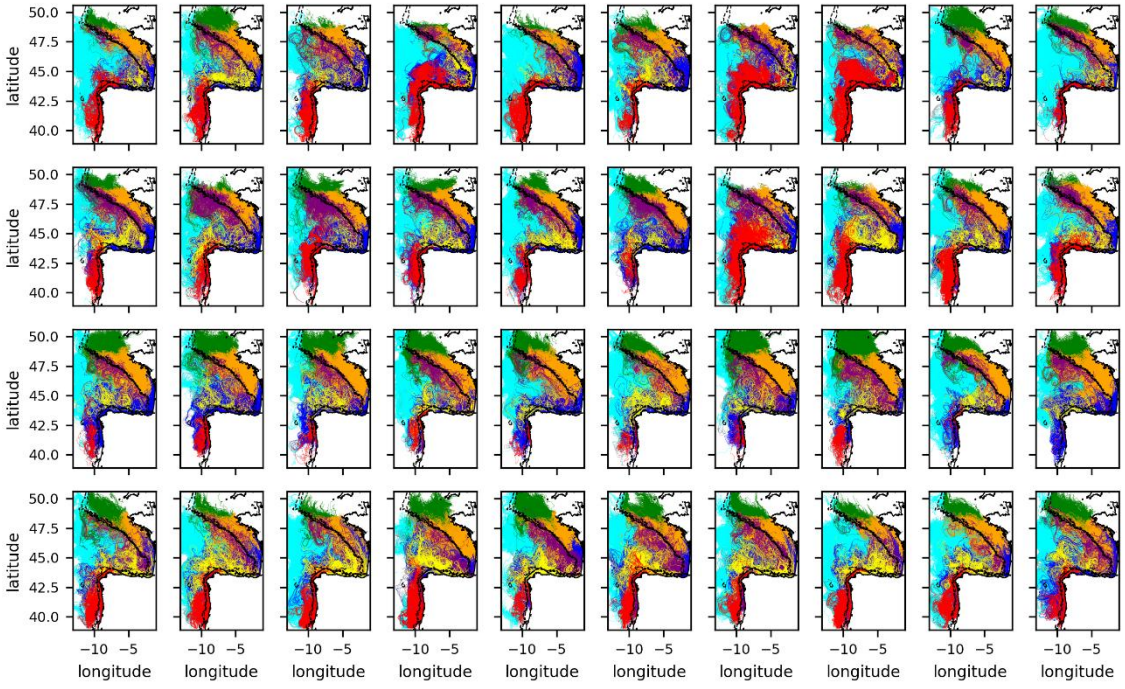

Figure A2: 90 days of backward trajectories of numerical particles seeded throughout February (upper row), May (second row), August (third row) and November (last row) for 2004 – 2013 (left to right). The trajectories are color-coded with their subareas of origin (as defined in Fig. 1) considering 90-days integration time. Contours show the 200 m and 1000 m isobaths.

https://doi.org/10.5194/egusphere-2026-4302
Preprint. Discussion started: 24 July 2026

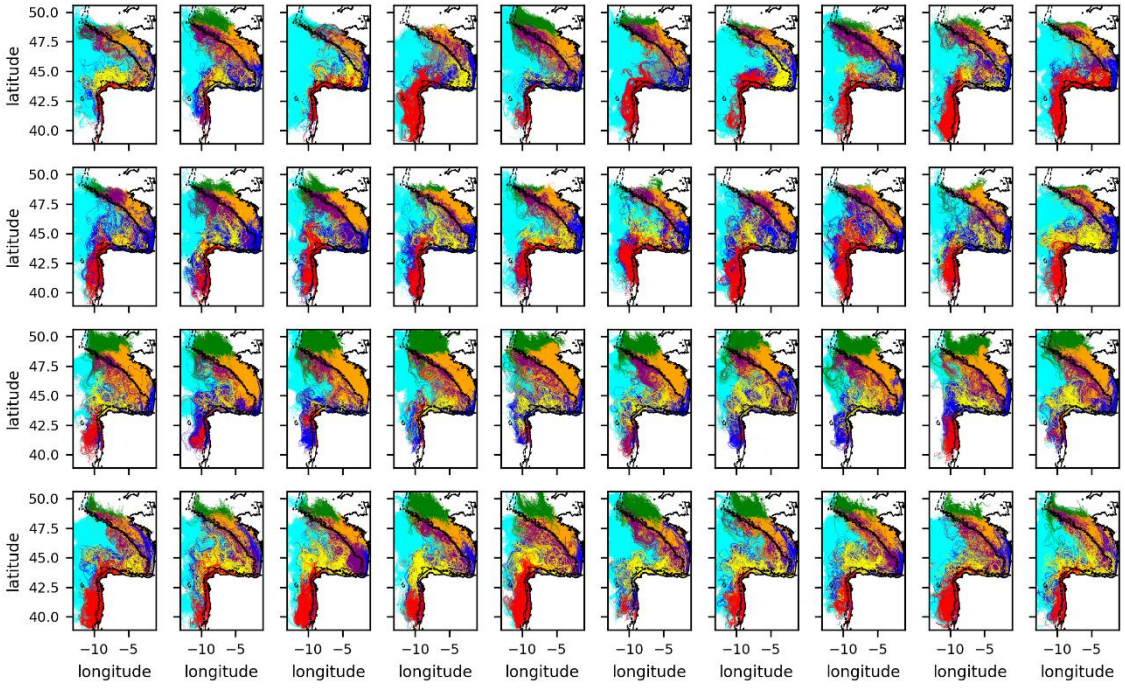

Figure A3: 90 days of backward trajectories of numerical particles seeded throughout February (upper row), May (second row), August (third row) and November (last row) for 2014 – 2023 (left to right). The trajectories are color-coded with their subareas of origin (as defined in Fig. 1) considering 90-days integration time. Contours show the 200 m and 1000 m isobaths.

https://doi.org/10.5194/egusphere-2026-4302
Preprint. Discussion started: 24 July 2026

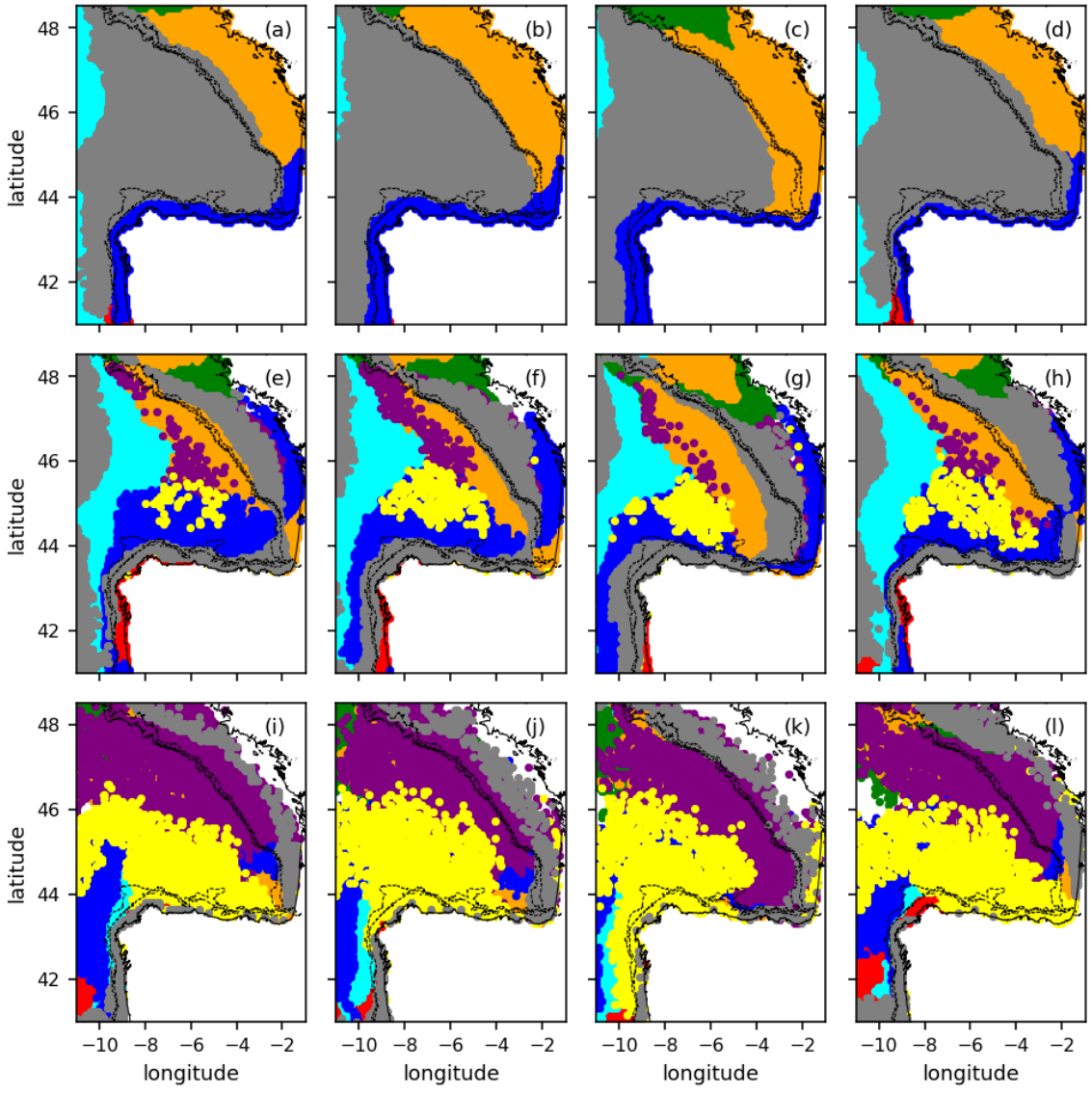

505 **Figure A4: Origin of particles at each seeding position for the first mode (a-d), second mode (e-h) and third mode (i-l) across the seven seedings per month and all simulated years for seedings in February (a,e,i), May (b,f,j), August (c,g,k) and November (d,h,l). Colours correspond to the origin of particles after 30-day backward simulations, according to the subareas as defined in Fig. 1. Light grey contours show the 200 and 1000 m isobaths.**

https://doi.org/10.5194/egusphere-2026-4302
Preprint. Discussion started: 24 July 2026

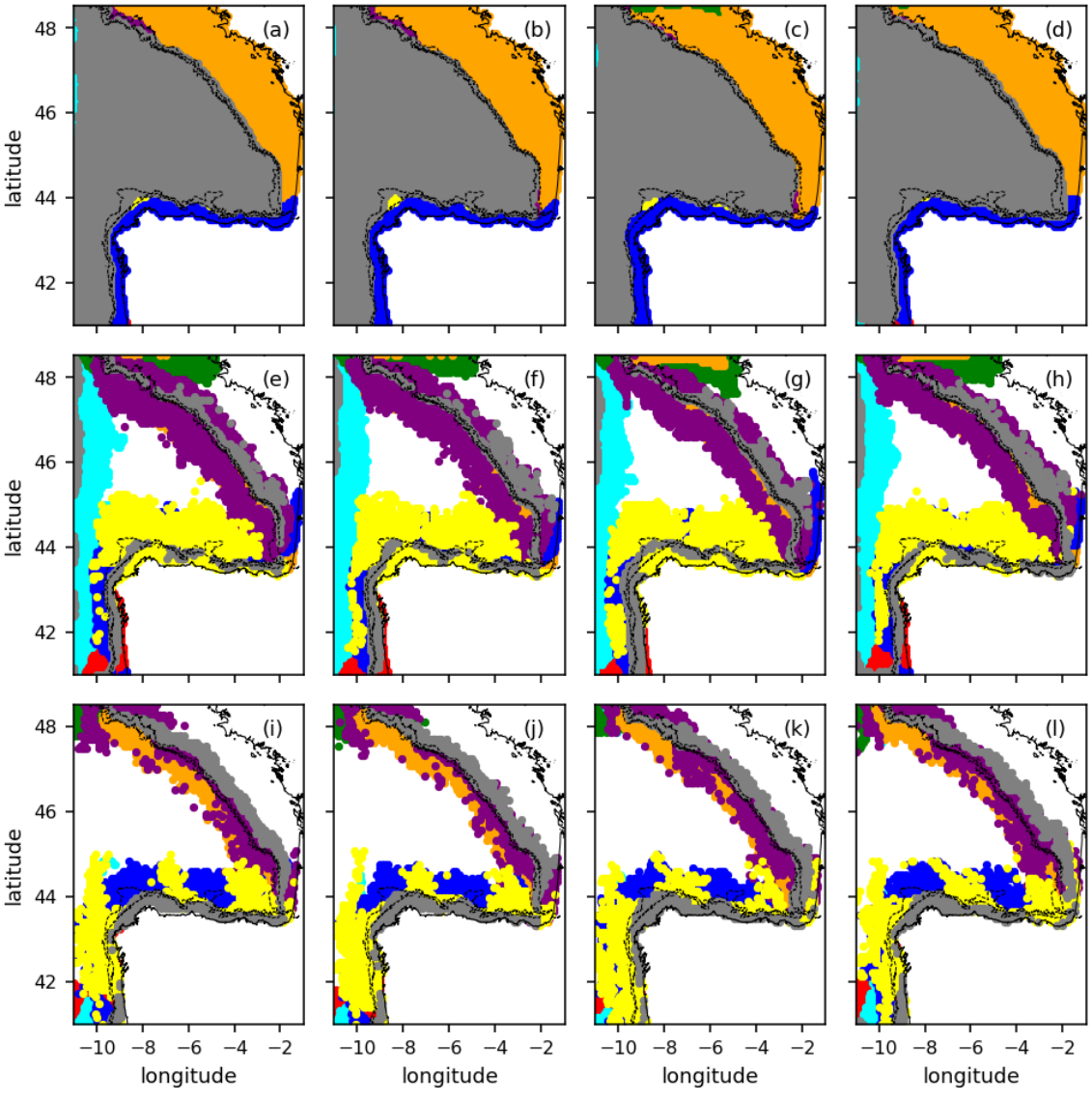

Figure A5: Origin of particles at each seeding position for the first mode (a-d), second mode (e-h) and third mode (i-l) across the seven seedings per month and all simulated years for seedings in February (a,e,i), May (b,f,j), August (c,g,k) and November (d,h,l). Colours correspond to the origin of particles after 7-day backward simulations, according to the subareas as defined in Fig. 1. Light grey contours show the 200 and 1000 m isobaths.

https://doi.org/10.5194/egusphere-2026-4302
Preprint. Discussion started: 24 July 2026

Code and data availability

All code used to run, process, and analyse the simulations was developed in Python using custom scripts and standard scientific packages, including NumPy, Xarray, and Matplotlib. The codes and the model output data will be made available following the FAIR principle once the manuscript is accepted for publication.

Author contributions

AR, AC and IM-N designed the experiments and NS carried them out. NS set up the model, performed the simulations and conducted most of the analysis with close guidance by all co-authors. All authors contributed to the generation of the manuscript.

Competing interests

The authors declare that they have no conflict of interest.

Disclaimer

Copernicus Publications remains neutral with regard to jurisdictional claims made in the text, published maps, institutional affiliations, or any other geographical representation in this paper. While Copernicus Publications makes every effort to include appropriate place names, the final responsibility lies with the authors. Views expressed in the text are those of the authors and do not necessarily reflect the views of the publisher.

Acknowledgements

This study has been conducted using E.U. Copernicus Marine Service Information; https://doi.org/10.48670/moi-00029 and OpenDrift (Dagestad et al 2018) version 1.13.0. AI tools were used to assist with language editing and text refinement, as well as for assistance in code development and troubleshooting. All generated content was reviewed and validated by the authors, who take full responsibility for the content of the manuscript.

Financial support

This project has received funding from the European Union's Horizon Europe research and innovation programme under the project BIOcean5D (award number 101059915) and co-Funded by the European Union. Views and opinions expressed are

https://doi.org/10.5194/egusphere-2026-4302
Preprint. Discussion started: 24 July 2026

however those of the author(s) only and do not necessarily reflect those of the European Union. Neither the European Union nor the granting authority can be held responsible for them. N. Steiger and A. Rubio have also received funding from the LAMARCA project (PID2021-123352OB-C31, C33) funded by MCIN/AEI/10.13039/501100011033 and by ERDF A way of making Europe.

References

Akpınar, A., Charria, G., Theetten, S., and Vandermeirsch, F.: Cross-shelf exchanges in the northern Bay of Biscay, J. Mar. Syst., 205, 103314, https://doi.org/10.1016/j.jmarsys.2020.103314, 2020.

Aldanondo, N., Cotano, U., Etxebeste, E., Irigoien, X., Alvarez, P., de Murguía, A. M., and Herrero, D. L.: Validation of daily increments deposition in the otoliths of European anchovy larvae (Engraulis encrasicolus L.) reared under different temperature conditions, Fish. Res., 93, 257–264, https://doi.org/10.1016/j.fishres.2008.04.012, 2008.

Aldanondo, N., Cotano, U., Tiepolo, M., Boyra, G., and Irigoien, X.: Growth and movement patterns of early juvenile European anchovy (Engraulis encrasicolus L.) in the Bay of Biscay based on otolith microstructure and chemistry, Fish. Oceanogr., 19, 196–208, https://doi.org/10.1111/j.1365-2419.2010.00537.x, 2010.

Alfaro-Ortega, C., Ibarretxe, J., and Iturrondobeitia, M.: Marine litter in the south-east of the Bay of Biscay: A review of current methods, standards, databases and challenges, Mar. Pollut. Bull., 213, 117632, 2025.

Amaro, T., Huvenne, V. A. I., Allcock, A. L., Aslam, T., Davies, J. S., Danovaro, R., De Stigter, H. C., Duineveld, G. C. A., Gambi, C., Gooday, A. J., Gunton, L. M., Hall, R., Howell, K. L., Ingels, J., Kiriakoulakis, K., Kershaw, C. E., Lavaleye, M. S. S., Robert, K., Stewart, H., Van Rooij, D., White, M., and Wilson, A. M.: The Whittard Canyon: A case study of submarine canyon processes, Prog. Oceanogr., 146, 38–57, https://doi.org/10.1016/j.pocean.2016.06.003, 2016.

Andruszkiewicz, E. A., Koseff, J. R., Fringer, O. B., Ouellette, N. T., Lowe, A. B., Edwards, C. A., and Boehm, A. B.: Modeling environmental DNA transport in the coastal ocean using Lagrangian particle tracking, Front. Mar. Sci., 6, 477, https://doi.org/10.3389/fmars.2019.00477, 2019.

Assis, J., Failler, P., Fragkopoulou, E., Abecasis, D., Touron-Gardic, G., Regalla, A., Sidina, E., Dinis, H., and Serrão, E. A.: Potential biodiversity connectivity in the network of marine protected areas in Western Africa, Front. Mar. Sci., 8, 765053, https://doi.org/10.3389/fmars.2021.765053, 2021.

Assis, J., Fragkopoulou, E., Serrão, E. A., and Araújo, M. B.: Coastal oceanographic connectivity at the global scale: A dataset of pairwise probabilities and travel times derived from biophysical modeling, Sci. Data, 12, 737, https://doi.org/10.1038/s41597-025-05060-2, 2025.

Atlantic-Iberian Biscay Irish-Ocean Physics Reanalysis: Copernicus Marine Service Marine Data Store, https://doi.org/10.48670/moi-00029, accessed 14 January 2026.

https://doi.org/10.5194/egusphere-2026-4302
Preprint. Discussion started: 24 July 2026

Ayata, S.-D., Pascal, L., and Thiebaut, E.: How does the connectivity between populations mediate range limits of marine invertebrates? A case study of larval dispersal between the Bay of Biscay and the English Channel (North-East Atlantic), Prog. Oceanogr., 87, 18–36, https://doi.org/10.1016/j.pocean.2010.09.022, 2010.

Balbar, A. C. and Metaxas, A.: The current application of ecological connectivity in the design of marine protected areas, Glob. Ecol. Conserv., 17, e00569, https://doi.org/10.1016/j.gecco.2019.e00569, 2019.

Basurko, O. C., Ruiz, I., Rubio, A., Beldarrain, B., Kukul, D., Cózar, A., Galli, M., Destang, T., and Larreta, J.: The coastal waters of the south-east Bay of Biscay a dead-end for neustonic plastics, Mar. Pollut. Bull., 181, 113881, https://doi.org/10.1016/j.marpolbul.2022.113881, 2022.

Bertin, S., Rubio, A., Hernández-Carrasco, I., Solabarrieta, L., Ruiz, I., Orfila, A., and Sentchev, A.: Coastal current convergence structures in the Bay of Biscay from optimized high-frequency radar and satellite data, Sci. Total Environ., 947, 174372, https://doi.org/10.1016/j.scitotenv.2024.174372, 2024.

Bertin, S., Rubio, A., Hernández-Carrasco, I., Orfila, A., and Sentchev, A.: The impact of windage on the transport and accumulation of marine litter: A Lagrangian analysis in the Bay of Biscay, J. Mar. Syst., 255, 104209, https://doi.org/10.1016/j.jmarsys.2026.104209, 2026.

Bjorkstedt, E. P. and Roughgarden, J.: Larval transport and coastal upwelling: An application of HF radar in ecological research, Oceanography, 10, 64–67, https://doi.org/10.5670/oceanog.1997.25, 1997.

Borja, A., Amouroux, D., Anschutz, P., Gómez-Gesteira, M., Uyarra, M. C., and Valdés, L.: The Bay of Biscay, in: World Seas: An Environmental Evaluation, 2nd ed., Academic Press, 113–152, https://doi.org/10.1016/B978-0-12-805068-2.00006-1, 2019.

Caballero, A., Pascual, A., Dibarboure, G., and Espino, M.: Sea level and eddy kinetic energy variability in the Bay of Biscay, inferred from satellite altimeter data, J. Mar. Syst., 72, 116–134, 2008.

Caballero, A., Ferrer, L., Rubio, A., Charria, G., Taylor, B. H., and Grima, N.: Monitoring of a quasi-stationary eddy in the Bay of Biscay by means of satellite, in situ and model results, Deep-Sea Res. Part II, 106, 23–37, https://doi.org/10.1016/J.DSR2.2013.09.029, 2014.

Caballero, A., Rubio, A., Ruiz, S., Le Cann, B., Testor, P., Mader, J., and Hernández, C.: South-eastern Bay of Biscay eddy-induced anomalies and their effect on chlorophyll distribution, J. Mar. Syst., 162, 57–72, https://doi.org/10.1016/j.jmarsys.2016.04.001, 2016.

Charria, G., Lazure, P., Le Cann, B., Serpette, A., Reverdin, G., Louazel, S., Batifoulier, F., Dumas, F., Pichon, A., and Morel, Y.: Surface layer circulation derived from Lagrangian drifters in the Bay of Biscay, J. Mar. Syst., 109–110, S60–S76, https://doi.org/10.1016/j.jmarsys.2011.09.015, 2013.

Cotano, U., Irigoien, X., Etxebeste, E., Alvarez, P., Zarauz, L., Mader, J., and Ferrer, L.: Distribution, growth and survival of anchovy larvae (Engraulis encrasicolus L.) in relation to hydrodynamic and trophic environment in the Bay of Biscay, J. Plankton Res., 30, 467–481, https://doi.org/10.1093/plankt/fbn011, 2008.

https://doi.org/10.5194/egusphere-2026-4302
Preprint. Discussion started: 24 July 2026

Cowen, R. K. and Sponaugle, S.: Larval dispersal and marine population connectivity, Annu. Rev. Mar. Sci., 1, 443–466, https://doi.org/10.1146/annurev.marine.010908.163757, 2009.

Dagestad, K.-F., Röhrs, J., Breivik, Ø., and Ådlandsvik, B.: OpenDrift v1.0: A modular framework for trajectory modelling, Geosci. Model Dev., 11, 1405–1420, https://doi.org/10.5194/gmd-11-1405-2018, 2018.

Declerck, A., Delpey, M., Rubio, A., Ferrer, L., Basurko, O. C., Mader, J., and Louzao, M.: Transport of floating marine litter in the coastal area of the south-eastern Bay of Biscay: A Lagrangian approach using modelling and observations, J. Oper. Oceanogr., 12 (Suppl. 2), S111–S125, https://doi.org/10.1080/1755876X.2019.1611708, 2019.

Drouet, K., Jauzein, C., Herviot-Heath, D., Hariri, S., Laza-Martinez, A., Lecadet, C., Plus, M., Seoane, S., Sourisseau, M., Lemée, R., and Siano, R.: Current distribution and potential expansion of the harmful benthic dinoflagellate Ostreopsis cf. siamensis towards the warming waters of the Bay of Biscay, North-East Atlantic, Environ. Microbiol., 23, 4956–4979, https://doi.org/10.1111/1462-2920.15406, 2021.

Fievet, G.-A., Boyra, G., Caballero, A., Manso-Narvarte, I., Martínez, U., Nieto, A., and Rubio, A.: Monitoring of anchovy schools by a glider-mounted echosounder in the south-eastern Bay of Biscay, Fish. Oceanogr., 2026.

Friocourt, Y., Levier, B., Speich, S., Blanke, B., and Drijfhout, S. S.: A regional numerical ocean model of the circulation in the Bay of Biscay, J. Geophys. Res.-Oceans, 112, C09008, https://doi.org/10.1029/2006JC003935, 2007.

Gaines, S. D., White, C., Carr, M. H., and Palumbi, S. R.: Designing marine reserve networks for both conservation and fisheries management, Proc. Natl. Acad. Sci. USA, 107, 18286–18293, https://doi.org/10.1073/pnas.0906473107, 2010.

González, M., Uriarte, A., Fontán, A., Mader, J. and Gyssels, P., "Marine dynamics." In *Elsevier Oceanography Series*, vol. 70, pp. 133-157. Elsevier, 2004

González-Pola, C., Somavilla, R., Graña, R., Viloria, A., and Ibáñez Tejero, L.: A decade long flow reversal in the intergyre region of the eastern North Atlantic, Prog. Oceanogr., 231, 103406, https://doi.org/10.1016/j.pocean.2024.103406, 2025.

ICES: Bay of Biscay and the Iberian Coast Ecoregion – Ecosystem Overview, ICES Advisory Report, https://doi.org/10.17895/ices.advice.7636, 2024.

Irigoien, X., Fiksen, Ø., Cotano, U., Uriarte, A., Alvarez, P., Arrizabalaga, H., Boyra, G., Santos, M., and Motos, L.: Could Biscay Bay anchovy recruit through a spatial loophole?, Prog. Oceanogr., 74, 132–148, https://doi.org/10.1016/j.pocean.2007.04.011, 2007.

Irigoien, X., Cotano, U., Boyra, G., Santos, M., Alvarez, P., Otheguy, P., Etxebeste, E., Uriarte, A., Ferrer, L., and Ibaibarriaga, L.: From egg to juvenile in the Bay of Biscay: Spatial patterns of anchovy (Engraulis encrasicolus) recruitment in a non-upwelling region, Fish. Oceanogr., 17, 446–462, https://doi.org/10.1111/j.1365-2419.2008.00492.x, 2008.

Koutsikopoulos, C. and Le Cann, B.: Physical processes and hydrological structures related to the Bay of Biscay anchovy, Sci. Mar., 60 (Suppl. 2), 9–19, 1996

Le Marchand, M., Hattab, T., Niquil, N., Albouy, C., Le Loc'h, F., and Ben Rais Lasram, F.: Climate change in the Bay of Biscay: Changes in spatial biodiversity patterns could be driven by the arrivals of southern species, Mar. Ecol. Prog. Ser., 647, 17–31, https://doi.org/10.3354/meps13401, 2020.

https://doi.org/10.5194/egusphere-2026-4302
Preprint. Discussion started: 24 July 2026

Lebreton, L. C.-M., Greer, S. D., and Borrero, J. C.: Numerical modelling of floating debris in the world's oceans, Mar. Pollut. Bull., 64, 653–661, https://doi.org/10.1016/j.marpolbul.2011.10.027, 2012.

Leis, J. M.: Behaviour as input for modelling dispersal of fish larvae: Behaviour, biogeography, hydrodynamics, ontogeny, physiology and phylogeny meet hydrography, Mar. Ecol. Prog. Ser., 347, 185–193, https://doi.org/10.3354/meps06955, 2007.

Lett, C., Verley, P., Mullon, C., Parada, C., Brochier, T., Penven, P., and Blanke, B.: A Lagrangian tool for modelling ichthyoplankton dynamics, Environ. Model. Softw., 25, 730–743, https://doi.org/10.1016/j.envsoft.2009.11.017, 2010.

Magris, R. A., Pressey, R. L., Weeks, R., and Ban, N. C.: Integrating connectivity and climate change into marine conservation planning, Biol. Conserv., 170, 207–221, https://doi.org/10.1016/j.biocon.2013.12.032, 2014.

Malauene, B. S., Lett, C., Marsac, F., Penven, P., Abdula, S., Moloney, C. L., and Roberts, M. J.: Influence of Mozambique Channel eddies on larval loss of two shallow-water commercial shrimp species, PLOS Clim., 3, e0000414, https://doi.org/10.1371/journal.pclm.0000414, 2024.

Manso-Narvarte, I., Caballero, A., Hernández-Carrasco, I., Orfila, A., Santos Mocoroa, M., Cotano, U., Jordà, G., Declerck, A., Delpey, M., and Rubio, A.: Effect of circulation at early life stages of European anchovy in the Bay of Biscay from observational data and a Lagrangian approach, J. Mar. Syst., 242, 103938, https://doi.org/10.1016/j.jmarsys.2023.103938, 2024.

Motos, L.: Reproductive biology and fecundity of the Bay of Biscay anchovy population (Engraulis encrasicolus L.), Sci. Mar., 60 (Suppl. 2), 195–207, 1996.

Nadal, I., Picciulin, M., Falcieri, F. M., García-Lafuente, J., Sammartino, S., and Ghezzo, M.: Spatio-temporal connectivity and dispersal seasonal patterns in the Adriatic Sea using a retention clock approach, Front. Mar. Sci., 11, 1360077, https://doi.org/10.3389/fmars.2024.1360077, 2024.

Paris, C. B., Cowen, R. K., Lwiza, K. M. M., Wang, D. P., and Olson, D. B.: Surfing, spinning, or diving from reef to reef: Effects on population connectivity, Mar. Ecol. Prog. Ser., 347, 285–300, https://doi.org/10.3354/meps06985, 2007.

Pingree, R. D. and Le Cann, B.: Anticyclonic eddy X91 in the southern Bay of Biscay, May 1991 to February 1992, J. Geophys. Res., 97, 14353–14367, https://doi.org/10.1029/92JC01181, 1992a.

Pereiro, D., Souto, C., and Gago, J.: Dynamics of floating marine debris in the northern Iberian waters: A model approach, J. Sea Res., 144, 57–66, https://doi.org/10.1016/j.seares.2018.11.007, 2019.

Prants, S. V.: Dynamical systems theory approach in oceanography: a review on achievements, limitations, verification and validation of Lagrangian methods, Front. Mar. Sci., 12, 1621820, https://doi.org/10.3389/fmars.2025.1621820, 2025.

Rubio, A., Caballero, A., Orfila, A., Hernández-Carrasco, I., Ferrer, L., González, M., Solabarrieta, L., and Mader, J.: Eddy-induced cross-shelf export of high Chl-a coastal waters in the SE Bay of Biscay, Remote Sens. Environ., 205, 290–304, https://doi.org/10.1016/j.rse.2017.10.037, 2018.

https://doi.org/10.5194/egusphere-2026-4302
Preprint. Discussion started: 24 July 2026

Ruiz, I., Abascal, A. J., Basurko, O. C., and Rubio, A.: Modelling the distribution of fishing-related floating marine litter within the Bay of Biscay and its marine protected areas, Environ. Pollut., 292, 118216, https://doi.org/10.1016/j.envpol.2021.118216, 2022a.

Ruiz, I., Rubio, A., Abascal, A. J., and Basurko, O. C.: Modelling floating riverine litter in the south-eastern Bay of Biscay: A regional distribution from a seasonal perspective, Ocean Sci., 18, 1703–1724, https://doi.org/10.5194/os-18-1703-2022, 2022b.

Serpette, A., Le Cann, B., and Colas, F.: Lagrangian circulation of the North Atlantic Central Water over the abyssal plain and continental slopes of the Bay of Biscay: Description of selected mesoscale features, Sci. Mar., 70 (Suppl. 1), 27–42, https://doi.org/10.3989/scimar.2006.70s127, 2006.

Solabarrieta, L., Rubio, A., Castanedo, S., Medina, R., Charria, G., and Hernández, C.: Surface water circulation patterns in the southeastern Bay of Biscay: New evidences from HF radar data, Cont. Shelf Res., 74, 60–76, https://doi.org/10.1016/j.csr.2013.11.022, 2014.

Teles-Machado, A., Peliz, Á., McWilliams, J. C., Dubert, J., and Le Cann, B.: Circulation on the Northwestern Iberian Margin: Swoddies, Prog. Oceanogr., 140, 116–133, https://doi.org/10.1016/j.pocean.2015.09.011, 2016.

Treml, E. A., Halpin, P. N., Urban, D. L., and Pratson, L. F.: The emergent geography of biophysical dispersal barriers across the Indo-West Pacific, Divers. Distrib., 21, 465–476, https://doi.org/10.1111/ddi.12307, 2015.

van der Kooij, J., et al.: Northward range expansion of BoB anchovy into the English Channel, Mar. Ecol. Prog. Ser., 741, 217–236, https://doi.org/10.3354/meps14603, 2024.

van Sebille, E., Aliani, S., Lavender Law, K., Maximenko, N., Alsina, J. M., Bagaev, A., Bergmann, M., Chapron, B., Chubarenko, I., Cózar, A., Delandmeter, P., Egger, M., Fox-Kemper, B., Garaba, S. P., Goddijn-Murphy, L., Hardesty, B. D., Hoffman, M. J., Isobe, A., Jongedijk, C. E., Kaandorp, M. L. A., Khatmullina, L., Koelmans, A. A., Kukulka, T., Laufkötter, C., Lebreton, L., Lobelle, D., Maes, C., Martinez-Vicente, V., Morales Maqueda, M. A., Poulain-Zarcos, M., Rodríguez, E., Ryan, P. G., Shanks, A. L., Shim, W. J., Suaria, G., Thiel, M., van den Bremer, T. S., and Wichmann, D.: The physical oceanography of the transport of floating marine debris, Environ. Res. Lett., 15, 023003, https://doi.org/10.1088/1748-9326/ab6d7d, 2020.

Wu, X., Voulgaris, G., and Kumar, N.: Shelf cross-shore flows under storm-driven conditions: Role of stratification, shoreline orientation, and bathymetry, J. Phys. Oceanogr., 48, 2533–2553, https://doi.org/10.1175/JPO-D-17-0090.1, 2018.